Models of fragmentations induced by electron attachment to protonated peptides

Vebjørn Bakken, Trygve Helgaker and Einar Uggerud*
Department of Chemistry, University of Oslo, PO Box 1033, Blindern, N-0315 Oslo, Norway.
E-mail: einar.uggerud@kjemi.uio.no

Invoking a number of theoretical levels ranging from HF/STO-3G to CCSD(T)/aug-cc-pVQZ, we have made a detailed survey of six potential energy surfaces (NH_4^+, $NH_4^\bullet$, $[CH_3CONHCH_3]H^+$, $[CH_3CONHCH_3]H^\bullet$, $[HCONHCH_2CONH_2]H^+$ and $[HCONHCH_2CONH_2]H^\bullet$). In conjunction with this, *ab inito* direct dynamics calculations have been conducted, tracing out several hundred reaction trajectories to reveal details of the electron-capture dissociation mechanism. The model calculations suggest the possibility of a bimodal pattern where some of the radicals, formed upon recombination, dissociate almost directly within one picosecond, the remaining radicals being subject to complete energy redistribution with a subsequent dissociation occurring at the microsecond timescale. Both processes give rise to *c* and *z* backbone fragments, resulting from cleavage of N–C_α bonds of the peptide chain.

Keywords: electron capture dissociation, mass spectrometry, proteomics, reaction dynamics, reaction mechanisms

Introduction

Due to its versatility, selectivity and sensitivity in protein identification and sequencing, mass spectrometry (MS) has become a key method in the field of proteomics.[1] Two methods are now used routinely for this purpose—namely, matrix-assisted laser desorption/ionization (MALDI)/MS[2,3] and elecrospray ionization (ESI)/MS.[4]

The relative molecular mass of a protein can be determined from the protonated molecule signal of the MALDI/MS spectrum, while amino acid sequence information can be inferred from ESI/MS. Before ESI/MS, the protein is cleaved into medium-sized peptides at specific positions using digestive enzymes—trypsin, for example, cleaves the backbone at the carboxylic side of peptide bonds associated with lysine and arginine residues.[5] The resulting peptide mixture can then be separated using high-performance liquid chromatography, whereupon the eluate is subject to ESI by which multiply-protonated peptides are fed successively into a mass analyzer. In a typical tandem mass spectrometry experiment, the molecule ions are first selected using a mass analyzer and energy is supplied to induce fragmentation of the selected ions. The resulting fragment ions are then identified using a second mass analyzer.

A common way to activate the decomposition of molecule ions is to collide them with a target gas in a cell situated in-line between the two mass analyzers [collisionally-induced decomposition, (CID)]. Usually, a doubly- or a triply-protonated molecule is selected using the first analyzer and the cleavages resulting from the collisional activation, typically, occur at the peptide C_O–N bonds. Depending on whether the proton that catalyzes the heterolytic peptide bond cleavage ends up on the carboxylic or the amino side, the fragment ion is called ***b*** or ***y***.[6,7] The mechanisms of these reactions are, by now, relatively well understood[8–13] and the series of ***b*** and ***y*** ions are used to determine the amino acid sequence of the peptide. Still, it is a limitation of this method that collisional activation does not induce fragmentation of all peptide bonds. Another problem with CID is that spectra are not reproducible between instruments. One important reason is that collison energies, depending on instrument type and setting, range from a few electronvolts to tens of kiloelectronvolts. The pressure and the nature of the target gas also have great influence on the appearance of the spectra.

An alternative and complementary activation method is, therefore, needed. A few years ago, Zubarev and McLafferty introduced a promising method, electron capture dissociation

DOI: 10.1255/ejms.665 ISSN 1356-1049

(ECD), in which the multiply-protonated peptide molecules are brought to interact with a bath of approximate thermal electrons.[14–16] During an ion/electron recombination process, the charge of the multiply protonated peptide is reduced by one, thereby releasing recombination energy and inducing cleavage of the peptide backbone. However, whereas CID breaks C_O–N bonds, ECD breaks N–C_α bonds, the resulting fragments being called ***c*** and ***z***. Moreover, the ECD process is more efficient than CID, cleaving most N–C_α bonds and giving rise to an almost complete series of sequence-specific ***c*** and ***z*** fragment ions. These facts point towards fast energy conversion and bond dissociation, in contrast to the relatively slow process of low-energy collisional activation and subsequent C_O–N bond cleavage in CID.

Two limiting mechanisms can be envisaged for ECD: a fast hydrogen atom cleavage mechanism (1) and a direct mechanism (2). Both mechanisms involve homolytic bond cleavage—see Scheme 1. Any actual mechanism is expected to be somewhere in-between these extremes. An intramolecular hydrogen bond from a protonation site (like R–NH_3^+) to the carbonyl group bridges the gap.

Storage-ring experiments have revealed that the hypervalent radicals that form upon electron recombination of H_3O^+ and NH_4^+ decompose to give free hydrogen atoms, providing support for Reaction 1(a) of Scheme 1.[17,18] However, as discussed below, this fact does not necessarily disprove Mechanism 2.

Model calculations employing reliable quantum chemical methods have provided some insight into the mechanism of ECD in particular[15,19,20] and into the chemistry of the type of radicals involved in general. The existing evidence favors electron capture, dissociation being faster than energy randomization in a molecule, pointing to a time scale of a few bond-vibration periods. This may imply a direct dissociation on a repulsive energy surface, a fast internal energy conversion that transfers vibrational energy into specific modes, or a vertical Franck–Condon process of the recombination event itself, with deposition of potential energy resulting from different equilibrium geometries of the ion and the neutral.

Since these mechanistic scenarios are of a dynamic nature, a complete theoretical treatment should not restrict itself to information on critical points of the potential energy surface (minima and saddle points) but incorporate the reaction dynamics explicitly. Therefore, we decided to investigate the ECD mechanism by combining static calculations of suitable peptide molecule ions and their radicals with reaction trajectory calculations.[21–24] Such calculations must be computationally feasible as well as physically realistic. We have chosen an approach that includes Hartree–Fock (HF) and density-functional theory (DFT) descriptions, combined with small to medium-sized basis sets. Model molecules that represent a portion of the peptide backbone containing five to seven main group atoms plus hydrogens were selected. It should be emphasized, however, that the models have been chosen to represent some relevant features of the ground state reaction dynamics of dissociating peptide radicals. This approach is, therefore, expected to give a qualitative insight into the chemical processes following recombination, rather than quantitative agreement with full-sized peptide ECD experiments.

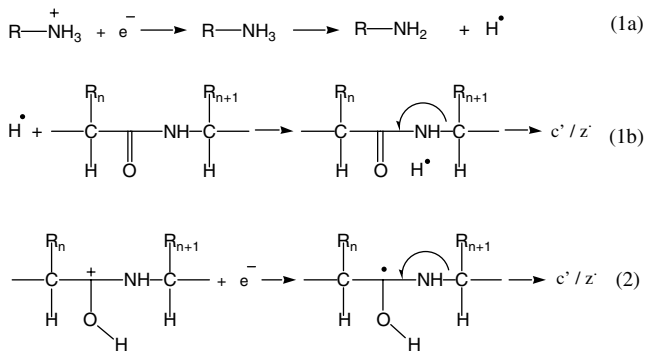

Scheme 1.

Methods

All quantum chemical calculations were carried out with Gaussian 98,[25] using HF theory[26] and Becke 3-parameter Lee–Yang–Parr (B3LYP)[27] DFT in the STO-3G,[28] 3-21G,[29] 4-31G,[30] 6-31G(d)[31] and aug-cc-pVDZ[32] basis sets. All stationary points were subject to a complete geometry optimization at the theoretical level used for the dynamic simulations, including a check for the correct number of negative Hessian eigenvalues. At this stage, analytical force constants were computed and the vibrational harmonic frequencies were obtained, together with the rotational constants. From these calculated spectroscopic constants, zero-point vibrational energies and thermochemical quantities were calculated within the rigid-rotor/harmonic-oscillator approximation. Geometries of stationary points may be obtained from the authors upon request.

The direct *ab initio* approach to trajectory calculations utilizes the first and second derivatives of the electronic energy with respect to atomic displacements (gradients and Hessians) to generate molecular trajectories $\boldsymbol{q}(t) = \{\boldsymbol{q}(t_1), \boldsymbol{q}(t_2), ...\}$ within the Born–Oppenheimer approximation.[21,22,33] For efficiency, the trajectory is calculated using a fifth-order predictor–corrector method, based on the repeated calculation of the wave function and its geometrical derivatives at points $\boldsymbol{q}_i$ in time steps, typically varying between 0.2 and 0.5 fs.[23,24] The energy and the molecular gradient are calculated at every point, whereas the Hessian is recalculated at every fifth point, being updated at the remaining points.

Direct dynamics is computationally demanding in that a single trajectory requires the calculation of the wave function and its derivatives at a large number of points. For this reason, there are severe limits on the complexity of the wave function that can be used. Typically, for each reaction and level of theory, we calculated 25–30 different trajectories,

Table 1. Energies (in Hartrees)[a].

Structure	HF	HF w/ZPVE	MP2(FC)	MP2(FC) w/ZPVE	CCSD(T)[b]
NH_4^+ (**1**)	–56.547984	–56.495548	–56.739780	–56.690107	–56.833186
NH_4@1 (**2´**)	–56.695839	–56.645836	–56.903118	–56.857109	not avail.
NH_4 (**2**)	–56.696051	–56.646871	–56.903932	–56.859771	–56.999417
NH_3 (**3**)	–56.205591	–56.169241	–56.404890	–56.370502	–56.495610
H (**4**)	–0.499334				–0.499948
TS ($NH_4 \rightarrow NH_3+H$)	–56.670893	–56.631585	–56.884020	–56.847759	–56.980512
NH_2 (**5**)	–55.575228	–55.554920	–55.728469	–55.709184	–55.813031
TS ($NH_3 \rightarrow NH_2+H$)	not avail.		–56.172121	–56.152454	–56.331929

[a]Basis set: aug-cc-pVDZ
[b]At MP2 geometry

which is a reasonable compromise between computer time, chemical accuracy and a representative ensemble of initial conditions taken from a thermal distribution.[34–36]

Results and discussion

In this section, we report the results of model calculations for reactions relevant to Scheme 1. Reaction 1 is discussed in the first (part a) and fourth (part b) sub-sections of this section, while the other sub-sections are devoted to variants of Reaction 2.

$$NH_4^+ + e^- \rightarrow NH_4 \rightarrow NH_3 + H$$

Even though a peptide is flexible so that protons migrate rapidly between its many basic sites, the protons tend to spend a large proportion of the time at the most basic sites, often at the nitrogens of the side chains of arginine, lysine and histidine. An essential feature of the upper mechanism of Scheme 1 is that it postulates that energetic hydrogen atoms are formed directly upon electron recombination in Equation [1(a)] (Scheme 1). The simplest model of a protonated basic side chain is the ammonium ion. We therefore decided to investigate the energetics and dynamics of dissociation of the NH_4 radical, formed upon electron capture. The small size

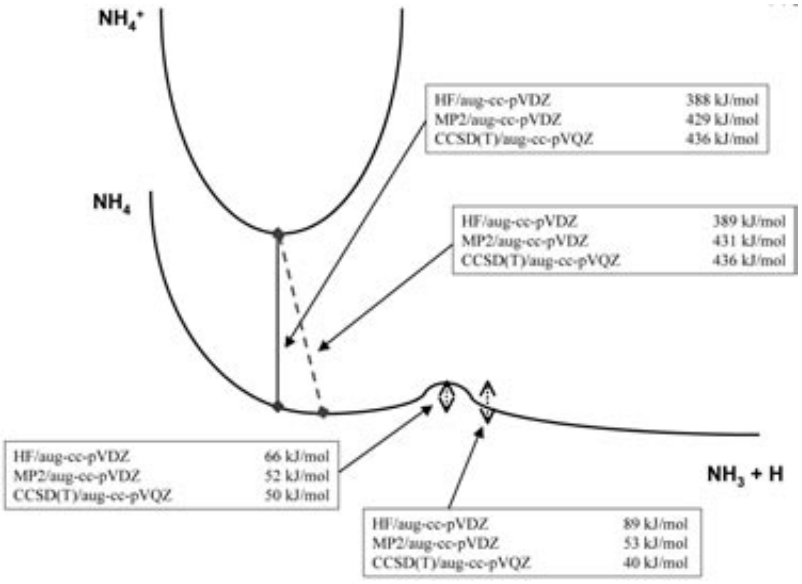

Figure 1. Schematic energy profile for the $NH_4^+/NH_4 \rightarrow NH_3 + H$ system. The vertical and adiabatic recombination energies are shown for several levels of theory, along with the forward and backward barriers for the dissociation. The CCSD(T)/aug-cc-pVQZ energies are calculated at the MP2/aug-cc-pVDZ geometries.

and the extensive literature on this system[18,37–50] combine to make this radical an attractive model system.

For our purposes, the HF/aug-cc-pVDZ model provides a good compromise between accuracy and cost. We calculated the vertical and adiabatic recombination energies to be 388 kJ mol^{-1} and 389 kJ mol^{-1}, respectively (Table 1, Figure 1). These values are in acceptable agreement with high-level CCSD(T)/aug-cc-pVQZ//MP2/aug-cc-pVDZ results (436 kJ mol^{-1} and 437 kJ mol^{-1}) as well as with existing experimental and theoretical results, which are in the range of 436–457 kJ mol^{-1}.[49,51,52] Since the ammonium ion represents an electronically closed octet, the ground-state of NH_4 radical resides in a shallow potential well, with a single electron in a quasi 3s orbital. The dissociation

$$NH_4\,(\mathbf{2}) \rightarrow NH_3\,(\mathbf{3}) + H\,(\mathbf{4}) \qquad (3)$$

is swift due to the low barrier, with a lifetime of 12 ps as estimated from the experiment.[46] A comparison shows that the HF/aug-cc-pVDZ model provides a good description by reproducing the shape of the CCSD(T)/aug-cc-pVQZ//MP2/aug-cc-pVDZ potential energy curve (Table 1). The forward barriers are 66 kJ mol^{-1} (HF) and 50 kJ mol^{-1} (CCSD(T)//MP2), the reverse barriers being 41 kJ mol^{-1} and 40 kJ mol^{-1}. These values agree well with the previous high-level study. Moreover, our study shows that the inclusion of diffuse basis functions is critical for an accurate description.

Since little is known about the details of the recombination process from the experiment, we will base much of our analysis on the theoretical description. The study of Park revealed a manifold of Rydberg states above the electronic ground state, all of which are stable towards dissociation.[49] Any dissociation must, therefore, occur from the ground state. In the following, we investigate two such scenarios.

In the first scenario, the initial conditions on NH_4^+ were chosen by random sampling of the rotational and vibrational degrees of freedom at a temperature of 298 K, whereupon the charge is changed from +1 to 0 and the dynamic development followed as a function of time. We would like to emphasize that from this mathematical sampling procedure in each case the molecule is given a fixed energy and there is no subsequent exchange of energy with the surroundings. At 298 K there is little vibrational exitation. A molecule with these initial conditions represents a situation where the recombination energy is lost by radiation within 1 fs. Although this is a rather poor approximation to reality, it does constitute a well-defined and simple limiting situation. Except for the sampled vibrational and rotational energy, the only energy available is the Franck–Condon energy of relaxing NH_4^+ to the NH_4 equilibrium geometry. If sufficiently excited, the energy floats around in NH_4 until enough energy has been concentrated in a single NH stretching motion to cause dissociation.

Of the 100 HF/aug-cc-pVDZ trajectories, 36 dissociated within 500 fs. Half of the dissociations occurred within the first 50 fs, the rest took place between 50 and 500 fs, the maximum trajectory integration time. The distribution appears bimodal, with one part having its maximum within the 0–50 fs range (life time corresponding to less than one N–H stretch) and the other part corresponding to an exponential decay for 50–500 fs. Given more time than 500 fs, it is likely that more trajectories would give rise to dissociation. The kinetic energy of the hydrogen atom, measured at 10 Å product separation, varied from 84 to 116 kJ mol^{-1}, the average being 98 kJ mol^{-1}. There is little correlation between the 298 K sampled internal energy (average 141 kJ mol^{-1}) and the translational energy of the hydrogen atom.

The second scenario corresponds to a situation where no energy is lost by radiative processes, all being available for dissociation. We simulated this situation by sampling an ensemble of NH_4^+ ions at 7000 K, roughly corresponding to the recombination energy, with a subsequent reduction to the ground-state NH_4 molecule. Unavoidably, sampling at this high temperature gives a wide energy distribution, resulting in many NH_4 molecules with an energy significantly higher or lower than the recombination energy.

A total of 25 HF/aug-cc-pVDZ trajectories were run, 24 of which yielded the dissociation into ammonia and a hydrogen atom within 25 fs. A single trajectory resulted in three rather than two products: NH_2 (**5**) + H + H. The trajectories were not stopped until all fragments were at least 20 Å away from one another, allowing NH_3 time to dissociate further. The translational energy distribution of the hydrogen varies from 94 to 414 kJ mol^{-1} with 221 kJ mol^{-1} as median. This corresponds to about 50% of the available energy ending up in the hydrogen atom. When we leave out the five highest and the five lowest energies, the median becomes 199 kJ mol^{-1}.

Neither scenario is in full agreement with experimental data. The first scenario is at odds with the observation that, in addition to NH_3, electron recombination gives a substantial amount of NH_2. The calculated low-energy content is simply insufficient to promote NH_2 formation, which requires at least 286 kJ mol^{-1}, which is the value for the transition structure for H_2 loss calculated at the singles-and-doubles configuration-interaction level of theory.[50] In the case of two subsequent hydrogen losses, at least 455 kJ mol^{-1}, the bond dissociation enthalpy of ammonia,[52] must be available after the first hydrogen loss.

As in the first scenario, it is difficult to assess the experimental results from the second scenario. Thus, even though the experimental product branching factors are 0.69 for NH_3, 0.10 for $NH_2 + H_2$ and 0.21 for $NH_2 + 2H$,[18] we observed NH_2 in only one trajectory. However, we note that our sampling procedure is probably too primitive in the sense that the true energy distribution of metastable NH_4 is narrower than a Boltzmann distribution. Furthermore, the cut-off at 20 Å may prevent the observation of NH_2. Indeed, an investigation of the 24 trajectories yielding $NH_3 + H$ reveals that, after the loss of the first hydrogen and the subtraction of the zero-point energy of NH_3, as many as five of these trajectories have enough energy left to break another NH bond. Given more time, these trajectories should yield $NH_2 + 2H$ as the final products. Thus, keeping in mind the statistical uncer-

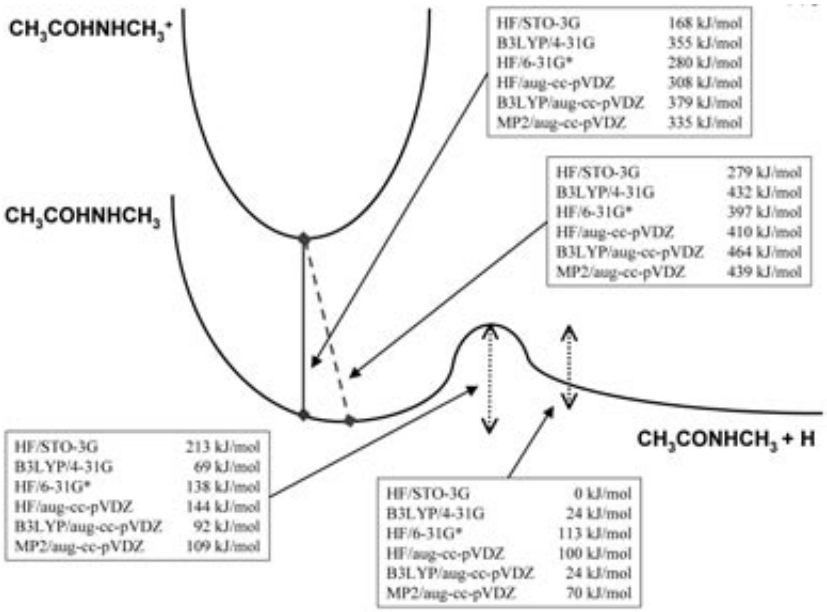

Figure 2. Schematic energy profile for the $CH_3COHNHCH_3^+/CH_3COHNHCH_3 \rightarrow CH_3CONHCH_3 + H$ system. The vertical and adiabatic recombination energies, as well as the forward and backward barriers for the dissociation, are shown for various combinations of wave functions and basis sets.

tainty, our simulation of the second scenario is in reasonable accordance with the experiment.

A second and probably equally important point is that we assume completely random phases of the vibrations. For example, if instead we had introduced the constraint of depositing the recombination energy into the totally symmetric molecular vibration (T_d), it is likely that we would have observed slightly longer NH_4 lifetimes and a somewhat different product distribution.

$CH_3C(OH)NHCH_3^+ + e^- \rightarrow CH_3C(OH)NHCH_3^\bullet$ and subsequent unimolecular dissociation

Syrstad *et al*. have studied this reaction both experimentally and theoretically.[20] High-level G2(MP2) calculations combined with RRKM theory reproduced the results of their neutralization/reionization experiments with protonated *N*-methyl-acetamide. Protonation on the carbonyl oxygen is thermochemically preferred. The two dominant unimolecular reactions of 1-hydroxy-1-(*N*-methyl)-aminoethyl radicals are the loss of the hydroxy hydrogen and the loss of the methyl group on the nitrogen, the latter corresponding to the ***c*/*z*** cleavages found for ECD. The former reaction dominates.

We have calculated the structures and energies of the key molecular species at different levels of theory—see Figure 2 and Table 2. With the exception of the crude HF/STO-3G level, the data obtained at the different levels are fairly consistent, with B3LYP/4-31G providing the most representative trajectories. For example, the barrier height for loss of the hydroxyl hydrogen atom is 69 kJ mol^{-1} with B3LYP/4-31G and 138 kJ mol^{-1} for HF/6-31G(d), compared with the

Table 2. Energies not including ZPVE (in Hartrees)[a].

Structure	HF/S	HF/L	HF/XL	B3LYP/M	B3LYP/XL	MP2/XL
$CH_3COHNHCH_3^+$ (**6**)	–244.302209	–247.362681	–247.403727	–248.547997	–248.911979	–248.194636
$CH_3COHNHCH_3$@**6** (**7′**)	–244.366071	–247.469218	–247.521201	–248.683163	–249.056157	–248.322297
$CH_3COHNHCH_3$ (**7**)	–244.408562	–247.513997	–247.559713	–248.712562	–249.088640	–248.361994
$CH_3CONHCH_3$ (**8**)	–243.861108	–247.006164	–247.043628	–248.195099	–248.560887	–247.847996
H (**4**)	–0.466582	–0.498233	–0.499334	–0.500273	–0.501657	–0.499334
TS (**7**→**8**+**4**)	–205.750005	–208.433124	–208.476153	–209.428485	–209.744660	–209.144145
CH_3COHNH (**9**)	–205.269896	–207.953327	–207.995051	–208.905706	–209.232833	–208.652373
CH_3 (**10**)	–39.077009	–39.558992	–39.565813	–39.788910	–39.844352	–39.698266
TS (**7**→**9**+**10**)	–244.341432	–247.470379	–247.516667	–248.679413	–249.056567	–248.314458

[a]Basis sets: S = STO–3G, M = 4-31G, L = 6-31G(d), XL = aug-cc-pVDZ

G2 value of 86 kJ mol^{-1}.[20] Note the presence of the reverse barrier for this process.

The initial conditions for our trajectories were selected from one ensemble at 298 K (corresponding roughly to an average of 428 kJ mol^{-1} sampled internal energy, 10 trajectories), one at 1000 K (516 kJ mol^{-1}, 10 trajectories) and one at 2000 K (719 kJ mol^{-1}, 20 trajectories). The simple HF/6-31G(d) wave function was employed, starting in all cases from $CH_3C(OH)NHCH_3^{\bullet}$ at the geometry of the ion. The integrations were stopped after 500 fs at 298 and 1000 K and after 1000 fs at 2000 K.

At the two lowest temperatures, no dissociation was observed. In contrast, at 2000 K, dissociation occurred for one half of the systems sampled. The *N*-methyl group was lost in three cases, with bond rupture occurring after about 200, 750 and 950 fs. In five cases, hydrogen was lost from the acetyl side to give $CH_2C(OH)NHCH_3$, all dissociations occurring within 300 fs and three within 100 fs. In one trajectory, a very hot hydrogen atom broke off from oxygen after just 100 fs. The fact that only one OH dissociation occurred, even though it is thermochemically preferable to CH dissociation, can be understood from the tighter transition structure of the former and from the HF/6-31G(d) overestimation of the OH dissociation barrier relative to G2.

Based on their G2 and RRKM calculations, Syrstad *et al*. concluded that, due to the favorable OH cleavage, $CH_3CONHCH_3/H^{\bullet}$ is not a fully realistic model of an ECD recombined protonated peptide. It is, therefore, somewhat paradoxical that, in our dynamical calculations, the simpler HF/6-31G(d) model predicts CH cleavage. Clearly, for a more realistic peptide model, it is necessary to extend the molecule on the acetyl side, as discussed later.

To investigate the dynamics of N–C_α bond dissociations, we conducted a series of calculations, starting from the transition state of the reaction leading to $CH_3C(OH)NH + CH_3$. Ten trajectories were run at the HF/6-31G(d) level, with rotations and vibrations sampled at 298 K. The transition mode was sampled thermally as a translation, the direction chosen so that CH_3 moved towards $CH_3C(OH)NH$. In this manner, the dissociation reaction ran "backwards", so as to investigate trajectories passing through the desired transition state and to see if this would lead to a hydrogen atom flying off from the oxygen.

In eight trajectories, the incoming CH_3 bonded to the nitrogen atom and remained stable within the integration limit of 500 fs. The two remaining trajectories lead to immediate recoil of the incoming CH_3. These were also run backwards by inverting the initial velocities, but this again produced $CH_3C(OH)NH + CH_3$. A total of 20 B3LYP/6-31G(d) trajectories were run at $T = 298$K, 15 of which gave $CH_3C(OH)NHCH_3$ stable for 500 fs. Four of the five remaining trajectories gave an immediate recoil of CH_3; in the last trajectory, the methyl group was bonded to nitrogen for a couple of C–N vibrational periods before departing.

$CH_3CONH_2CH_3^+ + e^- \rightarrow CH_3CONH_2CH_3^{\bullet}$ and subsequent unimolecular dissociation

To investigate how the initial position of the proton affects fragmentation, we also performed calculations on nitrogen-protonated *N*-methyl-acetamide. The initial conditions for the trajectory calculations were drawn from ensembles at 298 K, using HF/6-31G(d) (10 trajectories) and B3LYP/4-31G (20 trajectories), starting from $CH_3CONH_2CH_3^{\bullet}$ at the equilibrium geometry of the corresponding ion. All 30 trajectories resulted in rapid bond dissociation, in agreement with the potential energy diagram given in Figure 3.

Except for two B3LYP trajectories, all trajectories gave dissociation of the unstable C_O–N bond of the hypervalent species with formation of CH_3CO plus NH_2CH_3, corresponding to a ***b*/*y*** peptide cleavage. The remaining two

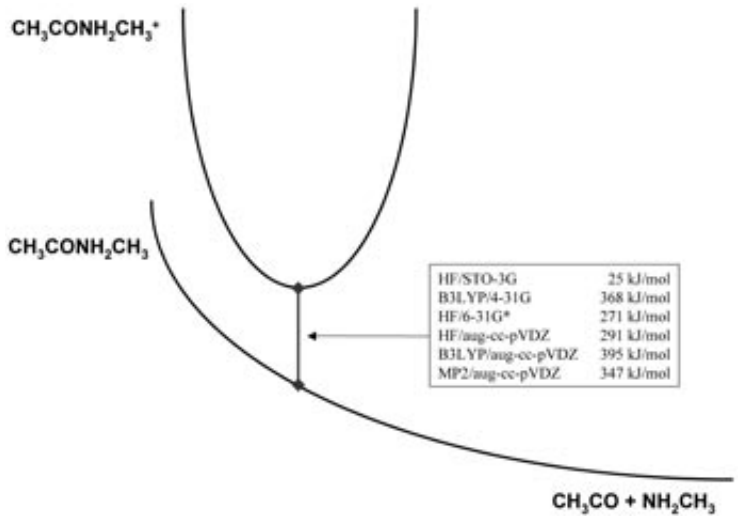

Figure 3. Schematic energy profile for the $CH_1CONH_2CH_3^+/CH_3CONH_2CH_3 \rightarrow CH_3CO + NH_2CH_3$ system. The vertical recombination energy is listed for several combinations of wave functions and basis sets.

B3LYP trajectories gave the products $CH_3CONHCH_3$ and $H^{\bullet}$. To gain more insight, the two latter trajectories were rerun, reversing the direction of integration to simulate an incoming hydrogen atom hitting the $CH_3CONHCH_3$ molecule at the nitrogen atom. Interestingly, both trajectories gave CH_3CO and NH_2CH_3 as products. As discussed below, these two trajectories can, in principle, represent the "hot" hydrogen model [Scheme 1, Reaction 1(b)]. However, as we shall see, random collisions with hot hydrogen atoms do not result in much fragmentation—in particular, ECD fragmentation. These reverse trajectories are unrepresentative, with improbable initial conditions, as will be evident from the forthcoming section.

We conclude that nitrogen-protonated peptides are not likely precursors for ECD, since $CH_3CONH_2CH_3^{\bullet}$ breaks up to give ***b*** and ***y*** rather than ***c*** and ***z*** fragments.

Bombardment of $CH_3CONHCH_3$ by H atoms of variable energies in random directions

The extreme variant of the so-called "hot" hydrogen model is depicted as a two-step process, where fast hydrogens resulting from recombination with ammonium sites liberate hydrogen atoms of considerable translational energy (Scheme 1). In our simulations of the simple NH_4 model, a mean translational energy corresponding to approximately one half of the available energy was found. To test the hypothesis that fast hydrogens are able to dissociate peptides, we conducted a series of dynamic simulations at different levels of theory, varying the translational energy of the hydrogen, the relative orientation and the impact parameter. In this respect, the translational energy is expected to be determining. Based on general chemical knowledge, thermal hydrogen atoms are, primarily, expected to abstract a hydrogen atom from a molecule or ion, with the formation of molecular hydrogen.

At the HF/STO-3G level, we sampled 25 initial situations at 298 K with random spatial orientations of the *N*-methyl-acetamide molecule, with the hydrogen atom 6 Å from the centre-of-mass, and sampling the impact parameter linearly in the range 0–3.5 Å. The integration of trajectories was repeated for the translational energies 72, 96 and 121 kJ mol^{-1}, giving a total of 75 trajectories for this wave function. The trajectories were run to a maximum separation of 10 Å or for a maximum duration of 500 fs.

With respect to energy conservation, these STO-3G trajectories were the most difficult to be carried out in this study. To avoid large energy jumps due to numerical instability, it was necessary to run some of the trajectories having a large impact parameter using extremely small step lengths. Clearly, this is an indication that the model has difficulties with describing the system properly. In fact, we observed that several electronic states came close in energy and even crossed along the reaction co-ordinate.

Most of the trajectories gave no reaction, the hydrogen atom hitting the amide and bouncing off, the collisions being slightly inelastic. At large impact parameters, we observed virtually no interaction. In one trajectory, the hydrogen atom attached to the oxygen atom; in three trajectories, it briefly bound to the carbonyl carbon atom. In four trajectories, the hydrogen atom bound to the carbonyl carbon atom of the peptide bond and remained there for the duration of the trajectory (500 fs). Even though these interactions weakened the neighboring C–N bond, no dissociation was observed. Finally, in three trajectories, the incoming hydrogen extracted a hydrogen atom from one of the methyl groups, forming a departing H_2 molecule.

The observed reaction pattern did not seem overly sensitive to the kinetic energy of the incoming hydrogen atom; trajectories with identical conditions except for the hydrogen translational energy behaved almost identically. To the extent that there was a difference in reactivity, it arose because hydrogen atoms of low kinetic energy take a longer time to reach the amide, allowing $CH_3CONH_2CH_3$ to reorient by internal rotation.

At the HF/6-31G(d) level, a total of 150 trajectories were run using the same approach to set up initial conditions as for HF/STO-3G, with 50 trajectories each for the hydrogen translational energies of 96, 144 and 192 kJ mol^{-1}, the impact parameter now being restricted to the range 0–2 Å (based on the experience from the minimal-basis trajectories). All trajectories were non-reactive with one exception, where the hydrogen atom bonded to oxygen and remained bonded throughout the 500 fs investigated. From the stationary points in Table 2, it is clear that the barrier to hydrogen addition is significantly higher for this basis set than for the other basis sets in the study.

Finally, 30 trajectories were examined at the B3LYP/4-31G level of theory. All trajectories were run by assigning 144 kJ mol^{-1} translational energy to the hydrogen atom. For those initial conditions that gave rise to a reaction (or looked very close to reacting), trajectories were also run with 96 kJ mol^{-1} and 192 kJ mol^{-1} translational energy, yielding a total of 44 trajectories at this level of theory. The trajectories were run for up to 500 fs or until the fragments were 10 Å apart.

The B3LYP/4-31G reaction pattern is similar to that found for HF/STO-3G. The hydrogen atom bonded to the oxygen atom in 12 trajectories—some remained stable for 500 fs, others ejected the hydrogen atom in the course of the simulation. The hydrogen atom also bonded to the carbonyl carbon in two trajectories; in one of these, the C–C bond was eventually broken, sending off a CH_3 radical. The other adducts remained stable for at least 500 fs. Again, the C–N bond was clearly weakened by the addition of the hydrogen atom, but no dissociation was observed at this bond. Four trajectories gave rise to H_2 by abstraction.

Despite some shortcomings in the wave functions used, it appears that incoming fast hydrogen atoms are likely to bounce off an amide/peptide rather than give rise to N–C fragmentation. The association of slow hydrogen atoms is out of the question because of the considerable barrier (Figure 2) as evident from the study of Syrstad and Turecek.

Table 3. Energies not including ZPVE (in Hartrees)[a].

Structure	HF/S	HF/L	HF/XL	B3LYP/M	B3LYP/XL	MP2/XL
$HCONHCH_2COHNH_2^+$ (**11**)	–371.304288	–376.103161	–376.169174	–377.754184	–378.322392	–377.308811
$HCONHCH_2COHNH_2$@**11** (**12′**)	–371.375087	–376.212698	–376.288648	–377.886112	–378.468139	–377.441706
$HCONHCH_2COHNH_2$ (**12**)	–371.382514	–376.261894	–376.334520	–377.922684	–378.505091	–377.483721
HCONH (**13**)	–166.107298	–168.297162	–168.326165	–168.969955	–169.236489	–168.783362
CH_2COHNH_2 (**14**)	–205.242420	–208.889677	–207.925823	–207.972539	–209.213081	–208.629657
TS (**12**→**13**+**14**)	–371.331860	–376.213098	–376.288079	–377.911787	–378.488163	–377.458715
$HCOHNHCH_2CONH_2^+$ (**15**)	–371.261782	–376.099442	–376.166070	–377.744892	–378.322283	–377.308131
$HCONHCH_2CONH_2$@**15** (**16′**)	–371.297175	–376.206463	–376.281474	–377.883443	–378.462902	–377.432487
$HCOHNHCH_2CONH_2$ (**16**)	–371.382000	–376.260909	–376.332704	–377.921475	–378.500062	?
HCOHNH (**17**)	–166.679160	–168.908008	–168.946023	–169.630486	–169.906192	–169.456132
CH_2CONH_2 (**18**)	–204.671960	–207.350073	–207.387999	–208.272110	–208.587743	–208.007042
TS (**16**→**17**+**18**)	–371.336836	–376.219621	–376.292681	–377.902638	–378.482671	–377.445414

[a]Basis sets: S = STO–3G, M = 4–31G, L = 6–31G(d), XL = aug-cc-pVDZ

The inability of polypetides to capture free hydrogen atoms has been demonstrated by Demirev.[53]

$HCONHCH_2C(OH)NH_2^+ + e^- \rightarrow HCONHCH_2C(OH)NH_2^\bullet$ and subsequent unimolecular dissociation

As noted above, *N*-methyl acetamide does not constitute a fully consistent peptide model for ECD. We therefore chose to investigate the larger $HCONHCH_2CONH_2$ model. An interesting feature of this peptide model is that the minimum potential energy form of the protonated molecule $HCONHCH_2C(OH)NH_2^+$ (**11**) has a hydrogen bond connecting the two carbonyl groups—see Table 3 and Figure 4 (left). The intramolecular $O–H^{(+)}\cdots O{=}C$ bond represents a stable situation, similar to the $N–H^{(+)}\cdots O{=}C$ bond between a protonated basic side group and a carbonyl oxygen of a peptide bond (Scheme 1). Using this model we believe we are in a better position to simulate a more realistic siuation in-between reactions 1 and 2 of Scheme 1.

Employing the HF/6-31G(d) level of theory, all rotational and vibrational degrees of freedom of the ion were sampled at 2000 K, before changing the charge from +1 to 0.

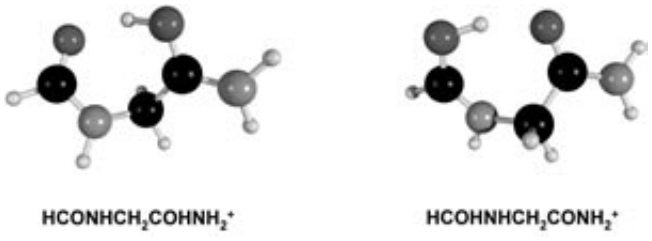

Figure 4. The lowest energy minima at the HF/6-31G* level for $HCONHCH_2COHNH_2^+$ (left) and $HCOHNHCH_2CONH_2^+$ (right).

In this manner, 30 trajectories were calculated. A complication arose because the lowest vibrational mode (~100 cm^{-1}) would be highly excited at the onset due to the statistics of the sampling procedure. Typically, there were more than ten vibrational quanta in this mode, challenging the harmonic approximation implicit in our initialization procedure. Ideally, this internal degree of freedom should be treated as an internal rotor. Lacking this option, it was decided to treat it as a translation, with the energy sampled thermally and the direction sampled randomly. This procedure underestimates the energy in the low-frequency mode somewhat but is preferable to a dramatic overestimation.

Out of the 30 trajectories run, 23 were non-reactive after 500 fs, the only significant change was that the hydrogen bond loosened and the molecule unfolded. Several of the trajectories reformed the loop for short periods. In five of the remaining seven trajectories, the hydrogen jumped immediately to the other oxygen before the loop opened. Previous quantum chemical calculations have shown that such processes are energetically facile.[54]

One of the two remaining trajectories gave an outcome of significance for the ECD process. After 200 fs, the N–C bond broke to give $HCOHNH + CH_2CONH_2$ as ***c/z*** fragments. It is particularly noteworthy that the intramolecular hydrogen transfer, which is prerequisite for forming the observed products, is immediate. As demonstrated by Turecek and Syrstad, intramolecular hydrogen transfer between two such oxygen atoms, typically, have a zero or low barrier.[54] From Table 3 and Figure 5, we infer that the complementary $HCONH + CH_2C(OH)NH_2$ products are higher in energy at all levels of theory. On the other hand, the barrier to forming these products, differing from ECD fragments only in the position of the radical, is slightly higher or slightly lower, depending on the level of theory. One could imagine that, if

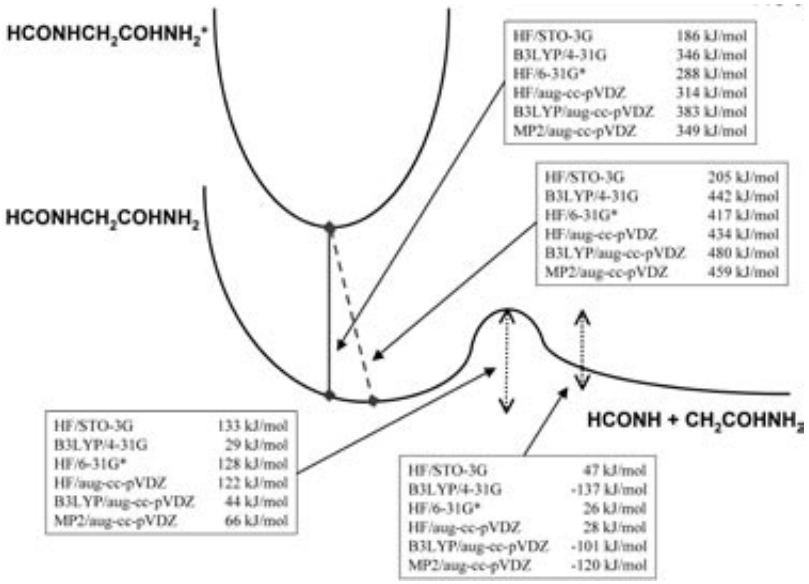

Figure 5. Schematic energy profile for the $HCONHCH_2COHNH_2^+$/$HCONHCH_2COHNH_2 \rightarrow HCONH + CH_2COHNH_2$ system. Vertical and adiabatic recombination energies are shown, along with the forward and backward barriers for the unimolecular dissociation.

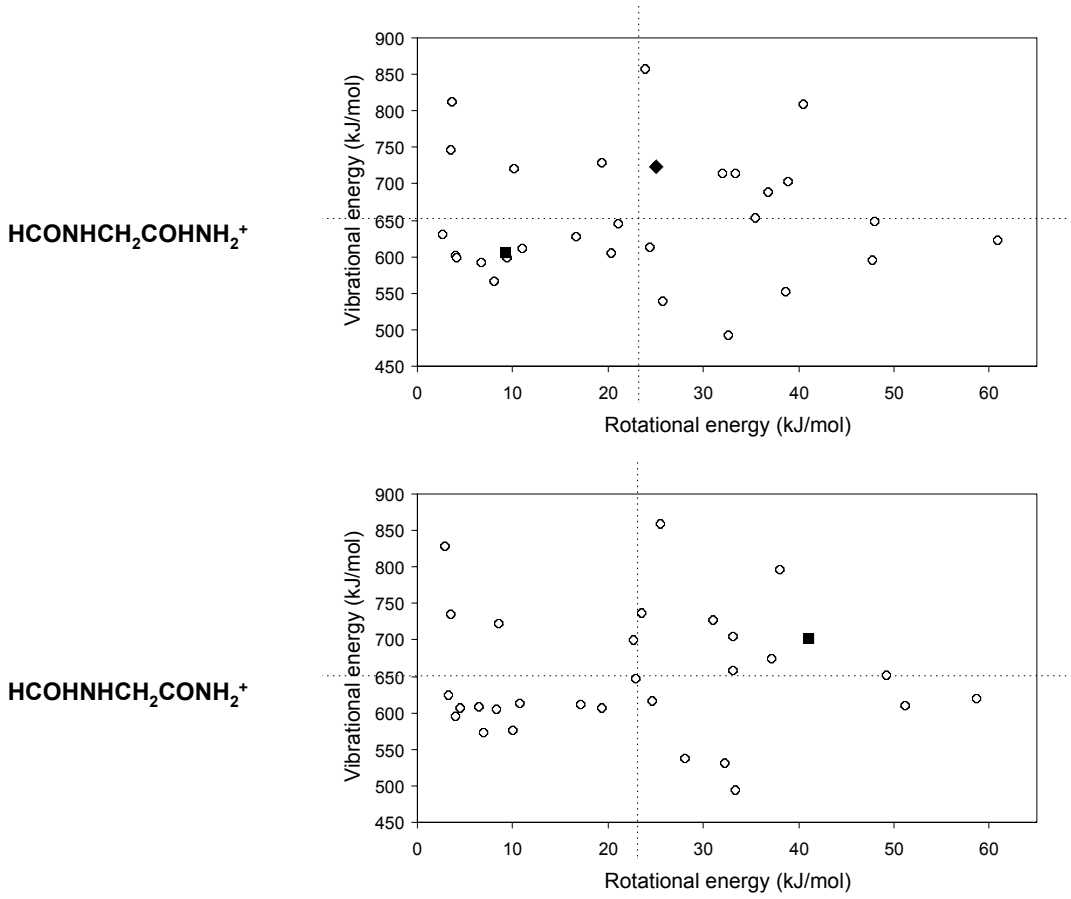

Figure 6. Sampled rotational and vibrational energy for $HCONHCH_2COHNH_2^+$ (upper plot) and $HCOHNHCH_2CONH_2^+$ (lower plot). The dashed lines represent the average sampled energies in each case. In the upper plot the solid diamond represents the initial sampled energies of the reactive trajectory $HCONHCH2COHNH_2 \rightarrow HCO + NHCH_2 + COHNH_2$, whereas the solid square represents the reactive trajectory $HCONHCH_2COHNH_2 \rightarrow HCOHNH + CH_2CONH_2$. In the lower plot the solid square represents the reactive trajectory $HCOHNHCH_2CONH_2 \rightarrow HCOHNH + CH_2CONH_2$.

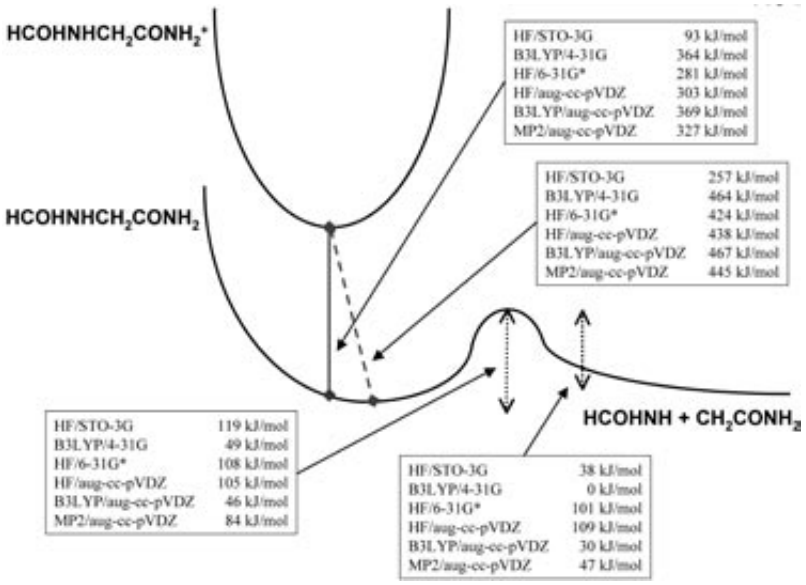

Figure 7. Schematic energy profile for the $HCOHNHCH_2CONH_2^+/HCOHNHCH_2CONH_2 \rightarrow HCOHNH + CH_2CONH_2$ system. Vertical and adiabatic recombination energies are shown, along with the forward and backward barriers for the unimolecular dissociation.

products of the higher energy type were formed in a long-chain peptide, there would be sufficient time for exothermic hydrogen atom transfer to give the more stable ECD products, owing to the high probability for entanglement of the two loose chains.

The single remaining trajectory resulted in a fast dissociation into three fragments $HCO + NHCH_2 + C(OH)NH_2$. Depending on the positions of the non-recombined charges of a long-chain peptide, this corresponds to ***a/x*** or ***b/y*** type products. It should be noted that the trajectories leading to peptide backbone fragmentations did not represent an exceptional internal energy content—see the upper panel of Figure 6.

$HC(OH)NHCH_2COHNH_2^+ + e^- \rightarrow HC(OH)NHCH_2COHNH_2^\bullet$ and subsequent unimolecular dissociation

From Table 3, we see that, for all higher level methods, $HC(OH)NHCH_2COHNH_2^+$ (**15**) is only marginally higher in energy than the isomer $HCONHCH_2C(OH)NH_2^+$ (**11**). The two isomers differ only in which oxygen atom is protonated, both forming loops from intramolecular $O–H^{(+)}\cdots O{=}C$ hydrogen bonds (Table 3, Figure 4 right). There is a similar small energy difference between the corresponding neutral radicals **16** and **12**, since the recombination energies are virtually identical.

As for the isomer in Reaction 5, we ran 30 HF/6-31G(d) trajectories with initial sampling at 2000 K, again with the lowest vibrational mode sampled as a translation. It is interesting to observe the similar behavior of the two isomeric systems. In the present case, $HC(OH)NHCH_2COHNH_2$ remained stable for 500 fs in 22 out of 30 trajectories, only displaying a loosening of the intramolecular hydrogen bond with subsequent unfolding. In five of the remaining trajectories, the hydrogen jumped to the other oxygen before the ring opened up. Furthermore, in two trajectories, the hydrogen broke off from oxygen (one from each oxygen) after 200–300 fs. A series of quantum chemical calculations have shown that the barrier to hydrogen loss is only slightly higher than that to hydrogen transfer.[54] Both of these trajectories were run backwards and again displayed exactly the same reaction at about the same time. Put together, these trajectories trace out a hydrogen atom visiting the peptide model for several hundred femtoseconds before flying off again.

Of all 30 trajectories, the most significant is the trajectory that produced HC(OH)NH and CH_2COHNH_2 after 450 fs, just as in the ECD backbone cleavage we are looking for. The observation of these fragments is understandable from Table 3 and Figure 7, noting that the HF/6-31G(d) barrier for this process is only $E_o = 108\,kJ\,mol^{-1}$ starting from $HC(OH)NHCH_2COHNH_2^\bullet$. For this type of N–$C_\alpha$ cleavage this value is rather large.[55] The average internal energy (the sum of the recombination energy, the zero-point vibrational energy and the original thermal vibrational energy) of the ensemble of $HC(OH)NHCH_2COHNH_2$ molecules obtained by the sampling process is $652\,kJ\,mol^{-1}$. Snapshots of the two dissociative trajectories are displayed in Figure 8.

To understand the kinetics of isomeric Reactions **5** and **6** better, we performed RRKM calculations of the reaction leading to the $HC(OH)NH + CH_2COHNH_2$ cleavage. Before discussing these results, we note that the reactive trajectories are by no means exceptional with regards to the sampled energy—see the lower panel of Figure 6.

Figure 9 displays the RRKM results as a rate curve. We note that an internal energy of $652\,kJ\,mol^{-1}$ corresponds to a rate coefficient of $3.9 \times 10^{11}\,s^{-1}$ and a half-life of 1.77 ps. The observation that three out of 60 trajectories led to decompo-

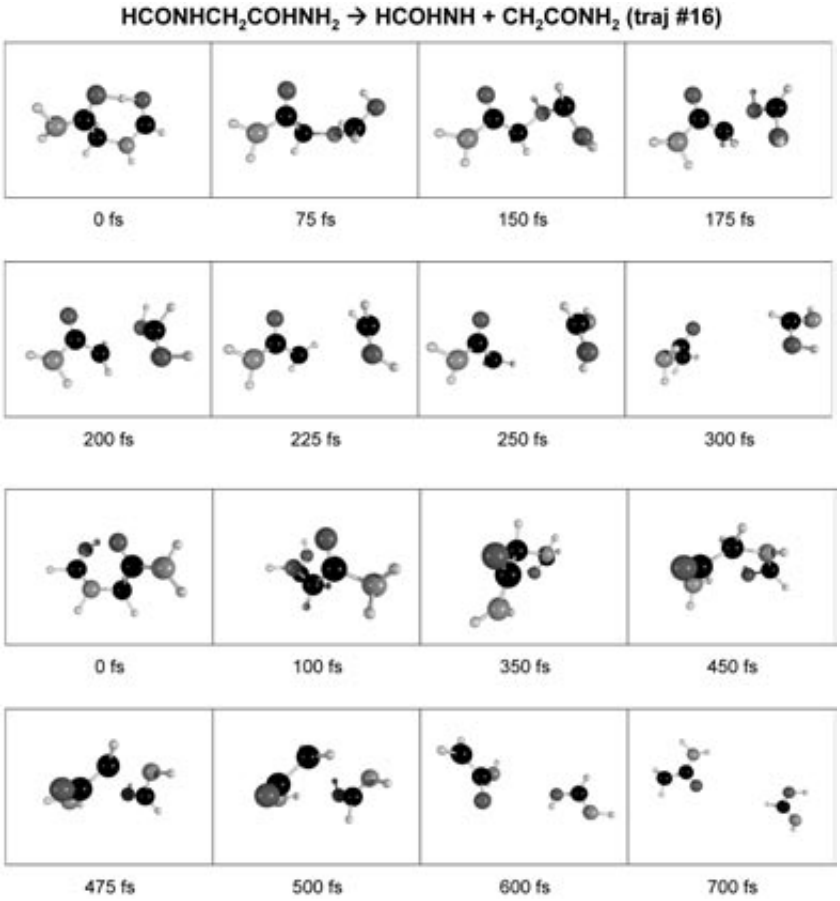

Figure 8. (a) Snapshots of the reactive trajectory $HCONHCH_2COHNH_2 \rightarrow HCOHNH + CH_2CONH_2$. (b) Snapshots of the reactive trajectory $HCOHNHCH_2CONH_2 \rightarrow HCOHNH + CH_2CONH_2$.

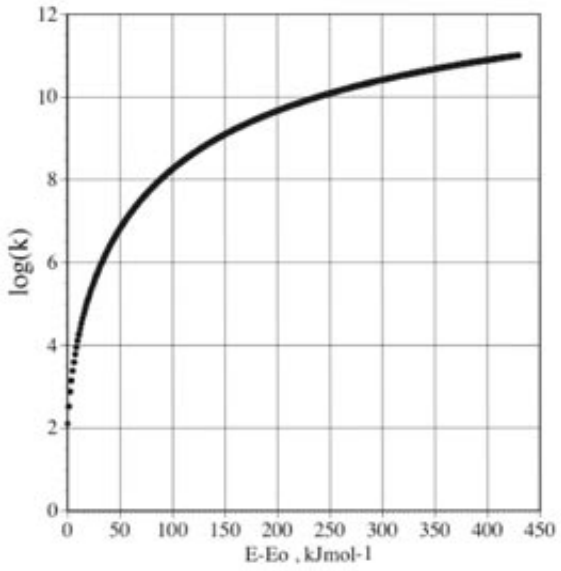

Figure 9. Logarithm of the rate coefficient, log *k*, plotted as function of the surplus energy, $E-E_o$, where E is the total energy and E_o is the critical energy of the dissociation $HCOHNHCH,CONH_2 \rightarrow HCOHNH + CH_2CONH_2$, obtained by RRKM as explained in

sition within 0.5 ps is, thus, in broad agreement with formal RRKM behavior in our model calculations. However, we also recognize the shortcomings of our models with respect to size. Lifetimes as short as 200–450 fs correspond to 6–15 C–C stretching vibrational periods, indicating that competition between intramolecular vibrational energy redistribution and dissociation starts to be significant.

Conclusion and perspectives

Our *ab inito* direct dynamics calculations have lead to several interesting conclusions.

We observe that loss of H upon recombination of NH_4^+ is accompanied by a substantial translational energy release (average 50% of recombination energy) and neither fast nor slow hydrogen atoms are efficient at dissociating the peptide backbone.

It was found that a hydrogen bonded to the carbonyl oxygen weakens the N–C_α bonds considerably. Furthermore, a realistic molecular model must encompass a situation where the protonation site (source of H radical) is "solvated" by a carbonyl oxygen. Our $[HCONHCH_2CONH_2]H^+$ model fulfils

this criterion. Using this model, a bimodal dissociation pattern is observed, where a quite small fraction of the radicals formed upon recombination dissociate within one picosecond.

It is natural to extrapolate the last point to bigger peptide molecules. Assuming that the energy is localized to a few atoms at or close to the radical site, we have shown that dissociation may occur at the femtosecond timescale. However, we have also observed that, for small molecules, those trajectories that do not result in disssociation within 1 ps instead lead to efficient intramolecular vibrational energy redistribution. This should be even more true for large molecules. For a peptide with several hundred well-coupled degrees of freedom, ergodic dissociation of a species with a weakened N–C_α bond would then occur on the timescale of milli- and microseconds rather than femto- and picoseconds, assuming initial conditions of the type studied here.

We emphasize that our model system does not provide quantitatively the ratio of femtosecond dissociation to intramolecular vibrational energy transfer, for the following two reasons: our incomplete knowledge regarding the exact initial conditions and the inaccurate barrier for dissociation energy of the N–C_α bond. The HF/6-31G(d) bond dissociation energy of 108 kJ mol^{-1} is reduced by 10 kJ mol^{-1} by including zero-point vibrations. In contrast, the corresponding B3LYP/aug-cc-pVDZ and MP2/aug-cc-pVDZ values are only 39 and 78 kJ mol^{-1}, respectively. Even lower barriers are possible in the case of amino acid residues, with alkyl or aryl substituents at the alpha carbon favoring femtosecond dissociation.

In conclusion, we have discussed a bimodal ECD mechanism— femtosecond dissociation in competition with internal vibrational relaxation (IVR) followed by slow dissociation. Our pictorial representation of the process is given in Figure 10. Further studies are needed to establish firmly the principal mechanism of the ECD process.

Acknowledgments

This work has received support through a grant of computer time from the Research Council of Norway (Grant No. NN1118K). The authors would also like to thank H. Bernhard Schlegel (Wayne State University) for the use of a development version of Gaussian 98.

References

1. J. Godovac-Zimmermann and L.R. Brown, "Perspectives for mass spectrometry and functional proteomics", *Mass Spectrom. Rev.* **20,** 1 (2001).
2. K. Tanaka, H. Waki, Y. Ido, S. Akita, Y. Yoshida and T. Yoshida, "Protein and polymer analysis up to *m/z* 100.000 by laser ionisation time-of-flight mass spectrometry", *Rapid Commun. Mass Spectrom.* **2,** 151 (1988).
3. M. Karas and F. Hillenkamp, "Laser desorption ionisation of proteins with molecular masses exceeding 10.000 daltons", *Anal. Chem.* **60,** 2299 (1988).
4. S.F. Wong, C.K. Meng and J.B. Fenn, "Multiple charging in electrospray ionization of poly(ethylene glycols)", *J. Phys. Chem.* **92,** 546 (1988).
5. J M. Berg, L. Stryer and J. Tymoczo, *Biochemistry*, 5th Edn. W.H. Freeman, San Fransisco, USA (2002).
6. P. Roepstorff and J. Fohlman, "Proposal for a common nomenclature for sequence ions in mass spectra of peptides", *J. Biomed. Mass Spectrom.* **11,** 601 (1984).

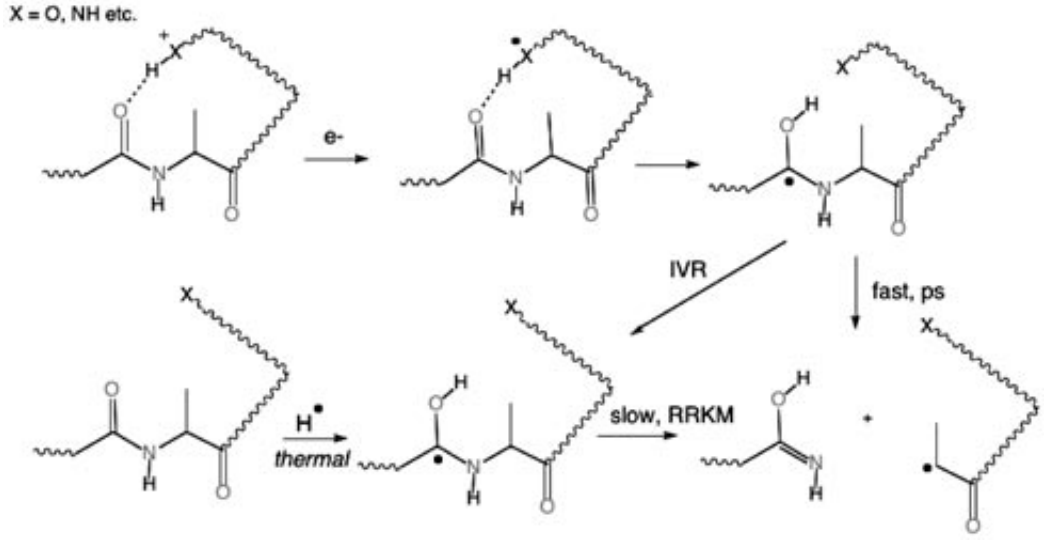

Figure 10. Schematics of suggested electron capture dissociation of a protonated peptide. The upper route corresponds to direct dissociation, while the lower routes assume complete energy resdistribution. In the latter case, the hydrogen atom may either be associated with the carbonyl initially after internal vibrational energy redistribution (IVR) or by trapping of a near-thermal hydrogen.

7. K. Biemann, "Contributions of mass spectrometry to peptide and protein structure", *Biomed. Environ. Mass Spectrom.* **16,** 99 (1988).
8. T. Yalcin, C. Khouw, I.G. Csizmadia, M.R. Peterson and A.G. Harrison, "Why are B ions stable species in peptide spectra?" *J. Am. Soc. Mass Spectrom.* **6(12),** 1165 (1995).
9. T. Yalcin, I.G. Csizmadia, M.R. Peterson and A.G. Harrison, "The structure and fragmentation of B_n (n 3) ions in peptide spectra", *J. Am. Soc. Mass Spectrom.* **7(3),** 233 (1996).
10. M.J. Nold, C. Wesdemiotis, T. Yalcin and A.G. Harrison, "Amide bond dissociation in protonated peptides. Structures of the N-terminal ionic and neutral fragments", *Int. J. Mass Spectrom. Ion Proc.* **164(1/2),** 137 (1997).
11. B. Paizs, G. Lendvay, K. Vekey and S. Suhai, "Formation of b_2^+ ions from protonated peptides: an *ab initio* study", *Rapid Commun. Mass Spectrom.* **13(6),** 525 (1999).
12. B. Paizs and S. Suhai, "Theoretical study of the main fragmentation pathways for protonated glycylglycine", *Rapid Commun. Mass Spectrom.* **15(8),** 651 (2001).
13. B. Paizs and S. Suhai, "Combined quantum chemical and RRKM modeling of the main fragmentation pathways of protonated GGG. II. Formation of b2, yl and y2 ions", *Rapid Commun. Mass Spectrom.* **16(5),** 375 (2002).
14. R.A. Zubarev, N.L. Kelleher and F.W. McLafferty, "Electron Capture Dissociation of Multiply Charged Protein Cations. A Nonergodic Process", *J. Am. Chem. Soc.* **120(13),** 3265 (1998).
15. R.A. Zubarev, N.A. Kruger, E.K. Fridriksson, M.A. Lewis, D.M. Horn, B.K. Carpenter and F.W. McLafferty, "Electron Capture Dissociation of Gaseous Multiply-Charged Proteins Is Favored at Disulfide Bonds and Other Sites of High Hydrogen Atom Affinity", *J. Am. Chem. Soc.* **121(12),** 2857 (1999).
16. R.A. Zubarev, D.M. Horn, E.K. Fridriksson, N.L. Kelleher, N.A. Kruger, M.A. Lewis, B.K. Carpenter and F.W. McLafferty, "Electron Capture Dissociation for Structural Characterization of Multiply Charged Protein Cations", *Anal. Chem.* **72(3),** 563 (2000).
17. L.H. Andersen, O. Heber, D. Kella, H.B. Pedersen, L. Vejby-Christensen and D. Zajfman, "Production of water molecules from dissociative recombination of H_3O^+ with electrons", *Phys. Rev. Lett.* **77(24),** 4891 (1996).
18. L. Vikor, A. Al-Khalili, H. Danared, N. Djuric, G.H.C. Dunn, M. Larsson, A. Le Padellec, S. Rosen and M. af Ugglas, "Branching fractions in the dissociative recombination of NH_4^+ and NH_2^+ molecular ions", *Astron. Astrophys.* **344,** 1027 (1999).
19. R.A. Zubarev, K.F. Haselmann, B. Budnik, F. Kjeldsen and F. Jensen, "Towards an understanding of the mechanism of electron-capture dissociation: a historical perspective and modern ideas", *Eur. J. Mass Spectrom.* **8(5),** 337 (2002).
20. E.A. Syrstad, D.D. Stephens and F. Turecek, "Hydrogen Atom Adducts to the Amide Bond. Generation and Energetics of Amide Radicals in the Gas Phase", *J. Phys. Chem. A* **107(1),** 115 (2003).
21. T. Helgaker, E. Uggerud and H.J.A. Jensen, "Integration of the Classical Equations of Motion on Ab Initio Molecular Potential Energy Surfaces using Gradients and Hessians: Application to Translational Energy Release upon Fragmentation", *Chem. Phys. Lett.* **173,** 145 (1990).
22. W. Chen, W.L. Hase and H.B. Schlegel, "Ab initio classical trajectory study of $H_2CO \rightarrow H_2+CO$ dissociation", *Chem. Phys. Lett.* **228,** 436 (1994).
23. J.M. Millam, V. Bakken, W. Chen, W.L. Hase and H.B. Schlegel, "Ab initio classical trajectories on the Born-Oppenheimer surface: Hessian-based integrators using fifth-order polynomial and rational function fits." *J. Chem. Phys.* **111,** 3800 (1999).
24. V. Bakken, J.M. Millam and H.B. Schlegel, "Ab initio classical trajectories on the Born–Oppenheimer surface: Updating methods for Hessian-based integrators", *J. Chem. Phys.* **111,** 8773 (1999).
25. M.J. Frisch, G.W. Trucks, H.B. Schlegel, G.E. Scuseria, M.A. Robb, J.R. Cheeseman, V.G. Zakrzewski, J.A. Mongomery, R.E. Stratmann, J.C. Burant, S. Dapprich, J.M. Millam, A.D. Daniels, K.N. Kudin, M.C. Strain, O. Farkas, J. Tomasi, V. Barone, M. Cossi, R. Cammi, B. Mennucci, C. Pomelli, C. Adamo, S. Clifford, J. Ochterski, G.A. Petersson, P.Y. Ayala, Q. Cui, K. Morokuma, D.K. Malick, A.D. Rabuck, K. Raghavachari, J.B. Foresman, J. Cioslowski, J.V. Ortiz, A.G. Baboul, B.B. Stefanov, G. Liu, A. Liashenko, P. Piskorz, I. Komaromi, R. Gomperts, R.L. Martin, D.J. Fox, T. Keith, M.A. Al-Laham, C.Y. Peng, A. Nanayakkara, C. Gonzalez, M. Challacombe, P.M.W. Gill, B.G. Johnson, W. Chen, M.W. Wong, J.L. Andres, A. Gonzales, M. Head-Gordon, E.S. Replogle and J.A. Pople, *GAUSSIAN 98*. Gaussian Inc. Pittsburgh, PA, USA (1998).
26. C.C.J. Roothan, "New Developments in Molecular Orbital Theory", *Rev. Mod. Phys.* **23,** 69 (1951).
27. A.D. Becke, "Density-functional thermochemistry. III. The role of exchange", *J. Chem. Phys.* **98,** 5648 (1993).
28. W.J. Hehre, R.F. Stewart and J.A. Pople, "Self-Consistent Molecular-Orbital Methods. I. Use of Gaussian Expansions of Slater-Type Atomic Orbitals", *J. Chem. Phys.* **51,** 2657 (1969).
29. J.S. Binkley, J.A. Pople and W.J. Hehre, "Self-Consistent Molecular Orbital Methods. 21. Small Split-Valence Basis Sets for First-Row Elements", *J. Am. Chem. Soc.* **102,** 939 (1980).
30. R. Ditchfield, W.J. Hehre and J.A. Pople, "Self-Consistent Molecular-Orbital Methods. IX. An Extended Gaussian-Type Basis for Molecular-Orbital Studies of Organic Molecules", *J. Chem. Phys.* **54,** 724 (1971).
31. M.J. Frisch, J.A. Pople and J.S. Binkley, "Self-consistent molecular orbital methods. 25. Supplementary functions for Gaussian basis sets", *J. Chem. Phys.* **80,** 3265 (1984).
32. R.A. Kendall, T.H. Dunning, Jr and R.J. Harrison, "Electron affinities of the first-row atoms revisited. Systematic basis sets and wave functions", *J. Chem. Phys.* **96,** 6796 (1992).
33. E. Uggerud and T.U. Helgaker, "The Dynamics of the Reaction: $CH_2OH^+ \rightarrow CHO^+ + H_2$. Translational Energy Release from Trajectory Calculations using an Ab Initio Potential Energy Function", *J. Anal. Chem. Soc.* **114,** 4265 (1992).
34. D.L. Bunker and E.A. Goring-Simpson, "Alkali-Methyl Iodide Reactions", *Faraday Discuss. Chem. Soc.* **55,** 93 (1975).
35. W.L. Hase and D.G. Buckowski, "Monte Carlo sampling of a microcanonical ensemble of classical harmonic oscillators", *Chem. Phys. Lett.* **74,** 284 (1980).

36. W.L. Hase, "Classical Trajectory Simulations: Initial Conditions", in *Encyclopedia of Computational Chemistry,* Ed by P.v.R. Schleyer, N.L. Allinger, T. Clark, J. Gasteiger, P.A. Kollmann, H.F Schaefer, III and P.R. Schreiner. John Wiley & Sons Ltd, Chichester, UK (1998).
37. J.K.S. Wan, "Is there a neutral ammonium radical", *J. Chem. Ed.* **45(1),** 40 (1968).
38. G. Gellene, D. Cleary and R. Porter, "Stability of the ammonium and methylammonium radicals from neutralized ion-beam spectroscopy", *J. Chem. Phys.* **77,** 3471 (1982).
39. H. Cardy, D. Liotard, A. Dargelos and E. Poquet, "Ab initio study of the thermodynamic and kinetic stability of the ammonium radical", *Chem. Phys.* **77(2),** 287 (1983).
40. G. Herzberg and J.T. Hougen, "Spectra of the ammonium radical: the Schuster band of deuterated ammonium radical", *J. Mol. Spectrosc.* **97(2),** 430 (1983).
41. S. Havriliak, T.R. Furlani and H.F. King, "Rydberg levels of the sodium atom and the ammonium radical calculated by perturbation theory", *Can. J. Phys.* **62(12),** 1336 (1984).
42. G. Herzberg, "Spectra of triatomic hydrogen and of the ammonium radical", *J. Mol. Struct.* **113,** 1 (1984).
43. J.K.G. Watson, W.A. Majewski and J.H. Glownia, "Assignment of the Schuster band of ammonia", *J. Mol. Spectrosc.* **115(1),** 82 (1986).
44. E. Kassab and E.M. Evieth, "Theoretical study of the ammoniated NH_4 radical and related structures", *J. Am. Chem. Soc.* **109(6),** 1653 (1987).
45. H. Cardy, D. Liotard, A. Dargelos, F. Marinelli and M. Roche, "Ab initio CI study of the emission spectrum and the vibronic coupling in the 3p2T2 state of the ammonium radical", *Chem. Phys.* **123(1),** 73 (1988).
46. K. Fuke and R. Takasu, "Ultrafast photochemistry of ammonia clusters: formation and decay of hypervalent molecular clusters containing the NH_4 radical", *Bull. Chem. Soc. Jpn* **68(12),** 3309 (1995).
47. J.M. Smith and W.A. Chupka, "Evidence for a deep Cooper minimum in the 3s-11p channel of ND_4", *Chem. Phys. Lett.* **250(5/6),** 589 (1996).
48. J.S. Wright and D. McKay, "Stability of the Rydberg Dimer $(NH_4)_2$", *J. Phys. Chem.* **100(18),** 7392 (1996).
49. J.K. Park, "Avoided curve crossing for the dissociation of the Rydberg NH_4 radical into (NH_3+H)", *J. Chem. Phys.* **107(17),** 6795 (1997).
50. J.K. Park, "Potential energy curves for the dissociation of the Rydberg NH_4 radical into (NH_2+H_2)", *J. Chem. Phys.* **109(22),** 9753 (1998).
51. M.W. Chase, Jr, C.A. Davies, J.R. Downey, Jr, D.J. Frurip, R.A. McDonald and A.N. Syverud, "JANAF Thermochemical Tables, 3rd Edn", *J. Phys. Chem. Ref. Data* **14(Supplement No. 1),** 1 (1985).
52. S.G. Lias, H.M. Rosenstock, K. Deard, B.W. Steiner, J.T. Herron, J.H. Holmes, R.D. Levin, J.F. Liebman, S.A. Kafafi, J.E. Bartmess, E.F. Hunter, P.J. Linstrom and W.G. Mallard, NIST webbook. *NIST Chemistry Webbook* (http://webbook.nist. gov/chemistry) 2002.
53. P.A. Demirev, "Generation of hydrogen radicals for reactivity studies in Fourier transform ion cyclotron resonance mass spectrometry", *Rapid Commun. Mass Spectrom.* **14(9),** 777 (2000).
54. F. Turecek and E.A. Syrstad, "Mechanism and Energetics of Intramolecular Hydrogen Transfer in Amide and Peptide Radicals and Cation Radicals." *J. Am. Chem. Soc.* **125,** 3353 (2003).
55. F. Turecek, "N–C, Bond Dissociation Energies and Kinetics in Amide and Peptide Radicals. Is the Dissociation a Non-ergodic Process?" *J. Am. Chem. Soc.* **125(19),** 5954 (2003).

Received: 27 April 2004
Revised: 12 August 2004
Accepted: 12 August 2004
Web Publication: 9 September 2004